Clin Exp Metastasis (2014) 31:435–446
DOI 10.1007/s10585-014-9638-5

RESEARCH PAPER

A humanized tissue-engineered in vivo model to dissect interactions between human prostate cancer cells and human bone

Parisa Hesami · Boris M. Holzapfel · Anna Taubenberger · Martine Roudier · Ladan Fazli · Shirly Sieh · Laure Thibaudeau · Laura S. Gregory · Dietmar W. Hutmacher · Judith A. Clements

Received: 21 November 2013 / Accepted: 15 January 2014 / Published online: 8 February 2014

Abstract Currently used xenograft models for prostate cancer bone metastasis lack the adequate tissue composition necessary to study the interactions between human prostate cancer cells and the human bone microenvironment. We introduce a tissue engineering approach to explore the interactions between human tumor cells and a humanized bone microenvironment. Scaffolds, seeded with human primary osteoblasts in conjunction with BMP7, were implanted into immunodeficient mice to form humanized tissue engineered bone constructs (hTEBCs) which consequently resulted in the generation of highly vascularized and viable humanized bone. At 12 weeks, PC3 and LNCaP cells were injected into the hTEBCs. Seven weeks later the mice were euthanized. Micro-CT, histology, TRAP, PTHrP and osteocalcin staining results reflected the different characteristics of the two cell lines regarding their phenotypic growth pattern within bone. Microvessel density, as assessed by vWF staining, showed that tumor vessel density was significantly higher in LNCaP injected hTEBC implants than in those injected with PC3 cells ($p < 0.001$). Interestingly, PC3 cells showed morphological features of epithelial and mesenchymal phenotypes suggesting a cellular plasticity within this microenvironment. Taken together, a highly reproducible humanized model was established which is successful in generating LNCaP and PC3 tumors within a complex humanized bone microenvironment. This model simulates

Electronic supplementary material The online version of this article (doi:10.1007/s10585-014-9638-5) contains supplementary material, which is available to authorized users.

P. Hesami · J. A. Clements (✉)
Australian Prostate Cancer Research Centre, Translational Research Institute, Queensland University of Technology, 37 Kent Street, Woolloongabba, QLD 4102, Australia
e-mail: j.clements@qut.edu.au
URL: www.australianprostatecentre.org

P. Hesami
e-mail: p.hesami@qut.edu.au

P. Hesami · B. M. Holzapfel · S. Sieh · L. Thibaudeau · D. W. Hutmacher (✉)
Regenerative Medicine Group, Institute of Health and Biomedical Innovation, Queensland University of Technology, 60 Musk Avenue, Kelvin Grove, QLD 4049, Australia
e-mail: dietmar.hutmacher@qut.edu.au

B. M. Holzapfel
e-mail: holzapfel@orthopaedic-oncology.net

S. Sieh
e-mail: s.sieh@qut.edu.au

L. Thibaudeau
e-mail: laure.thibaudeau@student.qut.edu.au

B. M. Holzapfel
Orthopedic Center for Musculoskeletal Research, University of Wuerzburg, Brettreichstr. 11, 97072 Würzburg, Germany

A. Taubenberger
Group of Cellular Machines, Biotec TU Dresden, Am Tatzberg 47-49, 01307 Dresden, Germany
e-mail: anna.taubenberger@biotec.tu-dresden.de

M. Roudier
Department of Pathology, University of Washington, Box 357470, Seattle, WA 98195, USA
e-mail: martineproudier@gmail.com

L. Fazli
Vancouver Prostate Centre, Department of Medicine, University of British Columbia, 2660 Oak Street, Vancouver, BC V6H 3Z6, Canada
e-mail: lfazli@prostatecentre.com

the conditions seen clinically more closely than any other model described in the literature to date and hence represents a powerful experimental platform that can be used in future work to investigate specific biological questions relevant to bone metastasis.

Keywords Tissue engineering · Prostate cancer · Bone metastasis · Osteotropism · Mouse model

Introduction

Prostate cancer (PCa) is the second most frequently diagnosed cancer worldwide [1] and the sixth leading cause of cancer death in males [2]. Bone metastases are found in about 75 % of patients with advanced PCa [3] and are a major cause of morbidity and mortality [4]. Symptoms and consequences associated with metastatic bone disease are highly debilitating and include intractable bone pain, increased fracture risk, spinal cord compression, bone marrow aplasia, hypercalcemia and leukoerythroblastic anemia [3, 5]. Currently for bone metastatic disease only palliative treatment options are available [3]. Despite its common occurrence, the reasons underlying the proclivity of PCa osteotropism remain poorly understood. To improve the treatment strategies that specifically target PCa bone metastasis, a better understanding of the interactions between PCa cells and bone is essential.

Several xenograft models have been described to study the interactions between human PCa cells and the bone microenvironment [6]. Traditional approaches include the injection of human PCa cells into the mouse tibia [7, 8] or into subcutaneously implanted human bone fragments [9–12]. In intratibial models, human PCa cells grow and interact with the mouse skeleton. This model is therefore not able to recapitulate the reciprocal interactions between human PCa cells and the human bone microenvironment. In the standard human bone chip model, human cancer cells are administered into subcutaneously implanted human bone fragments. This theoretically makes it possible to study species–specific interactions. However, this model does not sufficiently mimic the biological character of viable human bone as the implanted bone is poorly vascularized, necrotic and the trabecular spaces are mainly filled with fat cells and fibrotic tissue [6].

We hypothesized that the use of a humanized tissue-engineered bone construct (hTEBC) could overcome the limitations of traditionally used xenograft models of bone metastases. Our aim was to establish a model which is able to reconstitute a vascularized and viable humanized bone organ with a proliferative bone marrow compartment. This would better simulate the conditions seen in the clinic as PCa bone metastases are mainly found in the axial skeleton which is characterized by a high content of proliferative bone marrow. This novel model should be highly reproducible and should provide the possibility to monitor the amount and viability of the human cells implanted.

Although there are both osteolytic and osteoblastic lesions in PCa compared with, for example breast cancer bone metastasis which is predominantly osteolytic, it seems that bone metastasis in PCa tends to be more osteoblastic, appearing as focal areas of increased bone deposition or as osteosclerotic lesions characterized by bone formation [13, 14]. In this study, we used the well characterized LNCaP and PC3 PCa cell lines to establish tumors in these hTEBCs in vivo. The tumors formed by LNCaP are reported to be both osteolytic and osteoblastic (mixed lesion) but in general osteoblastic lesions dominate, whereas the PC3 tumors consist of osteolytic lesions without any surrounding osteogenic response [10]. Herein we describe a novel approach to engineer a viable humanized organ bone in vivo. Furthermore we extensively characterize the particular tumor phenotypes that grow in these bones when injecting LNCaP and PC3 cells. This model can be a highly attractive alternative to conventional models of bone metastasis when used to predict drug efficacy against a panel of human primary derived PCa tumors within a given histology.

Materials and methods

Animals

All animal experiments were conducted in conformity with the *Australian Code of Practise for the Care and Use of Animals for Scientific Purposes* and approved by the Queensland University of Technology Animal Ethics Committee (Approval number: 0900000102). Five week old male NOD/SCID mice were purchased from the Animal Resource Centre in Western Australia and kept under aseptic sterile conditions at the Biological Research Facility at the Princess Alexandra Hospital, Brisbane where they had

L. S. Gregory
Skeletal Biology Program, School of Biomedical Sciences, Queensland University of Technology, 60 Musk Avenue, Kelvin Grove, QLD 4059, Australia
e-mail: l.gregory@qut.edu.au

D. W. Hutmacher
George W Woodruff School of Mechanical Engineering, Georgia Institute of Technology, 801 Ferst Drive Northwest, Atlanta, GA 30332, USA

J. A. Clements
Cancer Program, Institute of Health and Biomedical Innovation, Queensland University of Technology, 60 Musk Avenue, Kelvin Grove, QLD 4059, Australia

access to food and water ad libitum. Animals were allowed to acclimatize for 1 week prior to the implantation of hTEBCs.

Prostate cancer cell lines and culture

PC3 and LNCaP PCa cell lines were obtained from the American Type Culture Collection (Rockville, MD). Cells were maintained in RPMI-1640 media (Invitrogen) supplemented with 10 % FBS and 1 % Penicillin/Streptomycin (Invitrogen) at 37 °C in 5 % CO_2.

Preparation of hTEBCs

Electrospun polycaprolactone scaffolds were gifts from the Guldberg Musculoskeletal Research Laboratory (George W. Woodruff School of Mechanical Engineering Parker H. Petit Institute of Bioengineering and Bioscience, Georgia Institute of Technology, Atlanta, US). Scaffolds were fabricated using a solution electrospinning technique as described by Kolambkar et al. [15]. Scaffolds had a cylindrical shape with a diameter of 4 mm and an approximate length of 5 mm. Meshes had 80–90 % porosity with pore sizes of 5–10 microns. Scaffolds were coated with calcium-phosphate (electrospun polycaprolactone calcium-phosphate; ePCL-CaP) to improve their biomimetic capacity [16].

Human osteoblasts (hOBs) were obtained after informed consent, from the femoral heads of patients undergoing total hip replacement as approved by the Ethics Committees of the Queensland University of Technology and the Prince Charles Hospital (Approval number: 0600000232). hOBs were isolated and cultured as previously described by our group [17]. Cells were expanded to passage four in α-MEM (Invitrogen) supplemented with 10 % FCS.

ePCL-CaP scaffolds were sterilized by washing with 70 % ethanol, drying and 20 min exposure to UV-light. Then, scaffolds were seeded with 2×10^5 hOBs. At day 4, the culture medium was replaced with osteogenic medium [α-MEM/10 % FCS supplemented with L-ascorbic acid-2-phosphate (50 μg/ml), β-glycerophosphate (10 mM) and dexamethasone (100 nm)]. Seeded scaffolds were cultured for 4 weeks and media was changed every 4–5 days. hOB cell sheets were prepared as previously reported [17]. Prior to implantation the hollow tubular scaffolds were loaded with a mixture of suspended hOBs, bone morphogenic protein-7 (BMP7) and fibrin glue (Fig. 1S; supplementary).

Characterization of seeded scaffolds

To validate the viability and morphology of the cells on the scaffolds, Fluorescein diacetate (FDA) and propidium iodide (PI) staining and Phalloidin–DAPI staining were performed according to previously described protocols [18]. Images were taken with a SP500 confocal laser scanning microscope (Leica) and presented as 3D projections. An Alizarin red S (Sigma-Aldrich) assay was performed as previously described [19] in order to demonstrate mineralization of the matrices.

Surgical procedures

General anaesthesia was induced with an i.p. injection of ketamine and xylazine (85 % saline: 10 % ketamine: 5 % xylazine with a dosage of 10 μl/g). hTEBCs were subcutaneously implanted in the right and left dorsal flank of 6-week old NOD/SCID mice. 12 weeks after implantation, PCa cell lines were injected transcutaneously into the implants. Each PCa cell line was suspended in sterile Growth Factor Reduced Matrigel Matrix (BD Biosciences) with 1×10^6 PC3 cells suspended in 30 μl Matrigel or 1×10^7 LNCaP cells suspended in 50 μl Matrigel. According to previous studies the take rate and volume of tumors formed by LNCaP is lower than PC3 tumors, therefore different numbers of PC3 and LNCaP cells were injected [10, 20]. Control mice received only 30 μl Matrigel. Mice were maintained for another 7 weeks before euthanasia. During this period, whole body weight and tumor dimensions were monitored. If weight loss was ≥15 % body weight at the time of injection and/or the tumor dimensions exceeded 1 cm^3, the animal was euthanized before the endpoint of the experiment. Implants were excised immediately post-mortem and were cleared from adjacent soft tissues. During necropsy tumor volume was calculated using the formula: Tumor volume $= \pi/6 \times a \times b^2$, where a is the longest dimension and b is the width [10]. Specimens were then fixed in 10 % neutral buffered formalin and transferred to 70 % ethanol the following day. There was no metastatic spread in any animal.

Micro-computed tomography (micro-CT) analysis

Micro-CT scans of the explanted hTEBCs were performed using a micro-CT 40 scanner (Scanco Medical, Switzerland) at a voxel size of 16 μm. Samples were evaluated at a threshold of 220 Gauss, a filter width of 0.8 and filter support of 1. X-ray attenuation was correlated to the sample density using a standard curve generated by scanning hydroxyapatite phantoms with known mineral density. The percentage of mineralized tissue volume to total tissue volume (MTV/TV) was quantified in each sample.

Histology

Following micro-CT imaging, specimens were decalcified using 10 % EDTA for 4 weeks. Fixed and decalcified hTEBCs were processed in a Thermo Scientific tissue processor (Excelsior ES). Samples were embedded in

paraffin (Thermo Scientific Shandon, Histocentre 3) and sectioned using a rotary microtome (Leica RM 2265) at a thickness of 5 μm. H&E staining was used to examine tissue structure and cell morphology. Two sections of each sample were analyzed, one from the central region of the implant and the other one 110 μm peripherally to the first section ($n = 5$ animals per group $\times$ 2 sections of each animal implant). All samples were analyzed by a specialist pathologist and tested for inter-observer and intra-observer variability.

Histochemistry

To detect osteoclasts, staining for tartrate-resistant acid phosphatase (TRAP) was performed as described previously [21] and counter-stained in Mayer's haematoxylin. Histomorphometric analyses were performed on the stained slides to quantify the osteoclasts per bone perimeter. Only multinucleated, TRAP-positive cells (red staining) on the bone surface were considered to be osteoclasts. Two sections of each sample were analyzed, one from the central region of the implant and the other one 110 μm peripherally to the first section. Using Osteomeasure (OsteoMetrics Inc., Atlanta, Georgia, USA) a random area of each section was selected to start measurements within a total area of 15 fields analyzed in each section. Bone perimeter and TRAP-positive osteoclast numbers were measured and the average number of osteoclasts along the bone perimeter (osteoclast surface) was calculated for statistical analysis.

Immunohistochemistry (IHC)

To block endogenous peroxidase activity, 3 % hydrogen peroxide was used for 30 min at room temperature. Proteinase K (Dako) for 30 min at room temperature was used to retrieve the antigens. To avoid non-specific antibody binding, samples were blocked with 2 % bovine serum albumin in PBS for 60 min at room temperature. The primary antibodies used were: Anti-NuMA (rabbit polyclonal anti-human NuMA, 1:100, EPITOMICS®, S2825), Anti-vWF (rabbit polyclonal anti-mouse von Willebrand Factor, 1:300, Millipore, AB7356), Anti-PTHrP (mouse monoclonal anti-human PTHrP, 1:140, Abcam, ab55631), Anti-E-Cadherin (mouse monoclonal anti-human, E-cadherin, 1:100, Invitrogen, 13-1700), Anti-vimentin (mouse monoclonal anti-human, vimentin, 1:100, Abcam, ab8069) Anti-osteocalcin (mouse monoclonal anti human, osteocalcin 1:200, Abcam, ab13420) and Anti-Collagen type II (mouse monoclonal anti-collagen type II, 1:200, DSHB, II-II6B3).

The slides were incubated with primary antibodies overnight at 4 °C in a humidified chamber. Non-immunized mouse or rabbit Immunoglobulin G (IgG) was used as an isotype control. The appropriate secondary antibody (Peroxidase-labelled dextran polymer conjugated goat anti-mouse and anti-rabbit immunoglobulins, DakoEnVision+Dual Link, Single Reagents, Dako Australia, K406189) was used. Color was developed using a peroxidase-based DAB substrate–chromogen solution (Dako K346889). Samples were then counter-stained with Mayer's haematoxylin.

To quantify the expression level of PTHrP, sections were scanned using a Nanozoomer slide scanner (Nanozoomer Digital Pathology System) and examined for two different areas (Implant: I and Tumor: T) by two independent investigators to account for inter-observer and intra-observer errors.

Blood vessel formation was quantified by examining the expression of vWF. To measure the microvessel density [22–24], slides were scanned using the Nanozoomer slide scanner and the blood vessels stained brown were counted in the entire section in the implant and tumor area at 20-fold magnification. The mean of each area from two different sections from the same hTEBC was then calculated for the microvessel density for each sample. Two sections, 110 μm apart from each other, were counted and averaged to calculate microvessel density for each animal. Data are presented as the number of blood vessels per field. The area of each field was 0.58 mm^2. PC3 cells directly interacted with the bone cells, and the tumor mass surrounded the hTEBC. Therefore, analyses were performed on the tumor (T) and implant (I) area in this group. However, in LNCaP tumors, there was not a direct contact between PCa cells and bone cells. Therefore only the tumor area was analyzed in this group.

Statistical analysis

Data were analyzed with SPSS (SPSS Statistics 19) using a linear mixed model with mice treated as a random effect. Independent t tests were performed to analyze differences between cell lines and control groups in each implant case. Results were considered significant at $p \leq 0.05$.

Results

Scaffold cell constructs were engineered and characterized as previously described (Fig. 1S) [25]. Prior to injecting the PCa cells, hTEBCs were analyzed at 7 and 12 weeks of implantation in mice using micro-CT and histology. Micro-CT indicated higher mineralized tissue volume to total volume (MTV/TV) in hTEBCs at 12 weeks compared with 7 weeks ($p = 0.043$) (Fig. 2S). Histology confirmed the presence of a bone organ including trabecular and cortical bone matrix, hematopoietic and fatty bone marrow (Fig. 3S). In mice euthanized at 7 weeks, a cartilage-like tissue (collagen type II positive) [26] which was surrounded by woven bone was observed (Fig. 3S) indicating

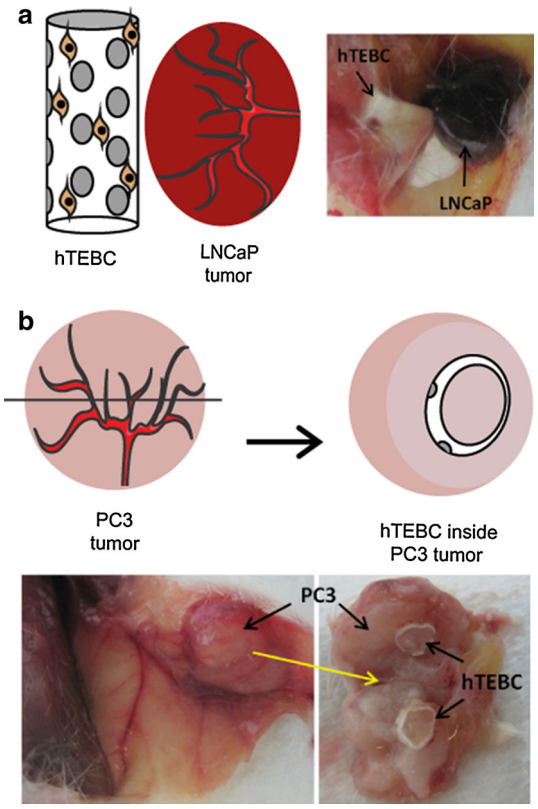

Fig. 1 Schematic of tumor growth using hTEBC and gross examination of the tumor masses during necroscopy after 19 weeks. **a** LNCaP tumors were formed adjacent to hTEBCs while **b** PC3 tumors formed inside and around the hTEBC. **a** LNCaP tumors had a *dark red* macroscopic appearance and tumor masses were mainly localized adjacent to the hTEBCs. **b** In contrast, PC3 tumors had a *light colour* and filled the bore of the cylinder

bone formation via the endochondral pathway. The bone matrix incorporated a large amount of human osteocytes as indicated by staining for human nuclear mitotic apparatus protein 1 (NuMa) (Fig. 4S).

PCa cells were injected 12 weeks after the implantation of hTEBCs, given the higher bone formation at this time point. At 19 weeks, the mice were euthanized. The frequency of tumor formation in hTEBCs was found to be 84 and 89 % after injection of PC3 and LNCaP cells, respectively. Mean tumor volume in hTEBCs was significantly higher in mice injected with PC3 cells (1×10^6) compared to mice injected with LNCaP cells (1×10^7) (PC3: 715.8 ± 93.8; LNCaP: 430.7 ± 98.6; $p = 0.01$). LNCaP tumors were dark red suggesting a high blood vessel density. In contrast, PC3 tumors were lighter in color suggesting either a solid viable tumor or a tumor rich in connective tissue. PC3 tumors surrounded the hTEBC while LNCaP tumors grew outside of it (Fig. 1).

As expected, quantitative evaluation of the MTV/TV was significantly lower in hTEBC implants injected with PC3 cells in comparison to the mice injected with LNCaP cells and Matrigel alone (control) ($p < 0.001$) (Fig. 2a). This was also clearly evident from the micro-CT 3D images showing the osteolytic effect of PC3 cells compared with LNCaP cells or Matrigel alone (Fig. 2b–d) as well as the histology results showing only a small amount of intact trabeculae in PC3-injected hTEBCs compared to solid trabeculae of bone in LNCaP-injected and control hTEBCs (Fig. 2e–g).

Histology results (H&E) confirmed a large amount of bone marrow in all experimental groups (Figs. 3, 4). In control and LNCaP-injected hTEBCs, a substantial amount of newly formed bone was observed (Fig. 3). Elements of hematopoietic bone marrow were present between the trabeculae. Trabecular bone in the form of small islands was usually present inside the construct in the bore of hTEBCs whereas cortical bone was surrounding the hTEBC forming a shell around it. Bone marrow was present within the cavity formed by the cortical bone (Fig. 3a, b). In hTEBCs injected with LNCaP cells, tumor growth was asymmetrical with a total growth to one side of the implant, with no direct contact with the hTEBCs and not filling the bore (Fig. 3c).The formation of lacunae and a large number of matrix-embedded osteocytes, indicative of viable bone, was observed in all cases (Figs. 3b, d, 4b). PC3-injected hTEBCs showed extensive osteolytic lesions with less amount of bone compared to LNCaP-injected and control hTEBCs (Figs. 3, 4). Only a small amount of bone was left 7 weeks after PC3 cell injection (Fig. 4a). Histological analysis confirmed the presence of osteolytic lesions with PC3 tumors (Fig. 4b).

In order to confirm the osteolytic effects observed histologically, TRAP staining was performed to detect osteoclasts. A large number of TRAP-positive osteoclasts were located in resorption pits at the surface of the trabeculae of PC3-injected and control hTEBCs (Fig. 5a, b) as well as LNCaP-injected hTEBCs (data not shown). TRAP staining for osteoclasts showed that the number of osteoclasts in hTEBC injected with PC3 cells was significantly higher than in the constructs injected with LNCaP cells ($p = 0.008$) or with the control vehicle ($p = 0.023$) (Fig. 5e) confirming the osteolytic behavior of PC3 cells.

Furthermore, immunostaining for anti-human anti-osteocalcin showed that strong osteocalcin expression was detected in the area of new bone formation (Fig. 5c). Osteocalcin is the major non-collagenous matrix protein expressed in bone [27]. It is considered a late and specific osteogenic marker whose expression is thought to be limited to mature osteoblasts [27]. Osteocalcin was also highly expressed in PC3 cells (Fig. 5c) as previously reported, whereas, it has been reported that LNCaP cells did not express osteocalcin [28].

PTHrP is a polypeptide hormone which is highly expressed by PCa tumors and is an osteoclast stimulatory factor [29]. Since PTHrP expression was evenly distributed, we used a conventional four-point scale scoring method in

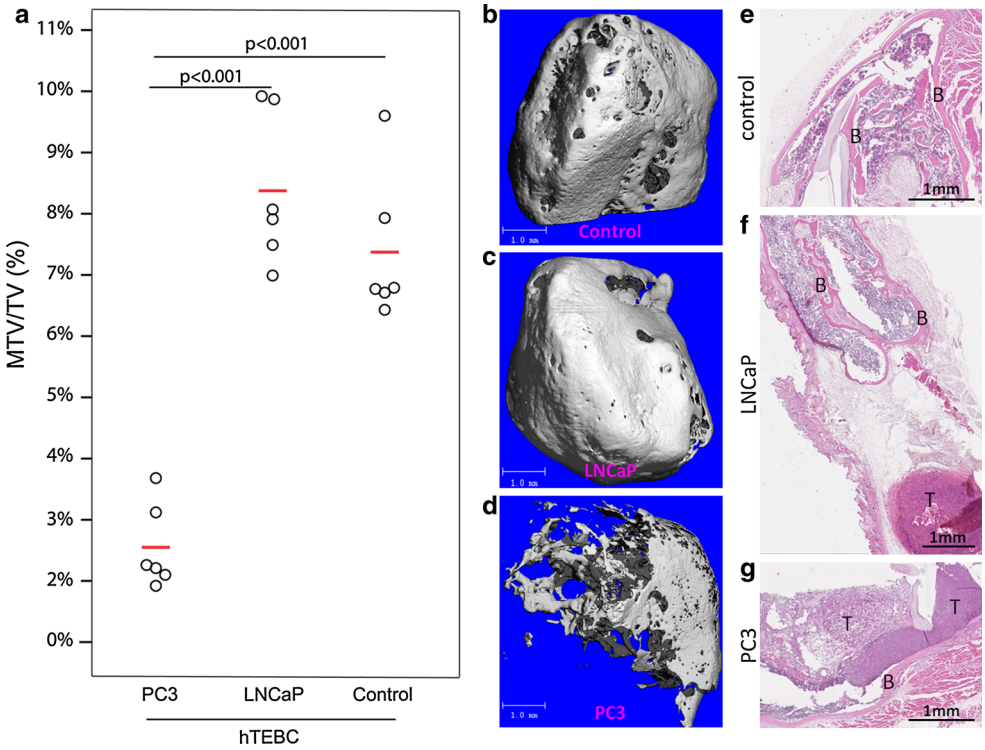

Fig. 2 Micro-CT and histology analysis of hTEBCs after 19 weeks. **a** Quantitative micro-CT analysis of the ossicles in the different groups ($n = 6$ per group) demonstrated a significantly lower mineralized tissue volume to total volume (MTV/TV) for the hTEBCs injected with PC3 cells. **b–d** Representative 3D images of hTEBCs in the different study groups showing the structural integrity of the ossicles in the control and the LNCaP group and a destruction of the cortical shell in the PC3 group. **e–g** Overview of the H&E staining of **e** hTEBC in the vehicle control mice, **f** hTEBC injected with LNCaP cells and **g** hTEBC injected with PC3 cells. *T* tumor, *B* bone

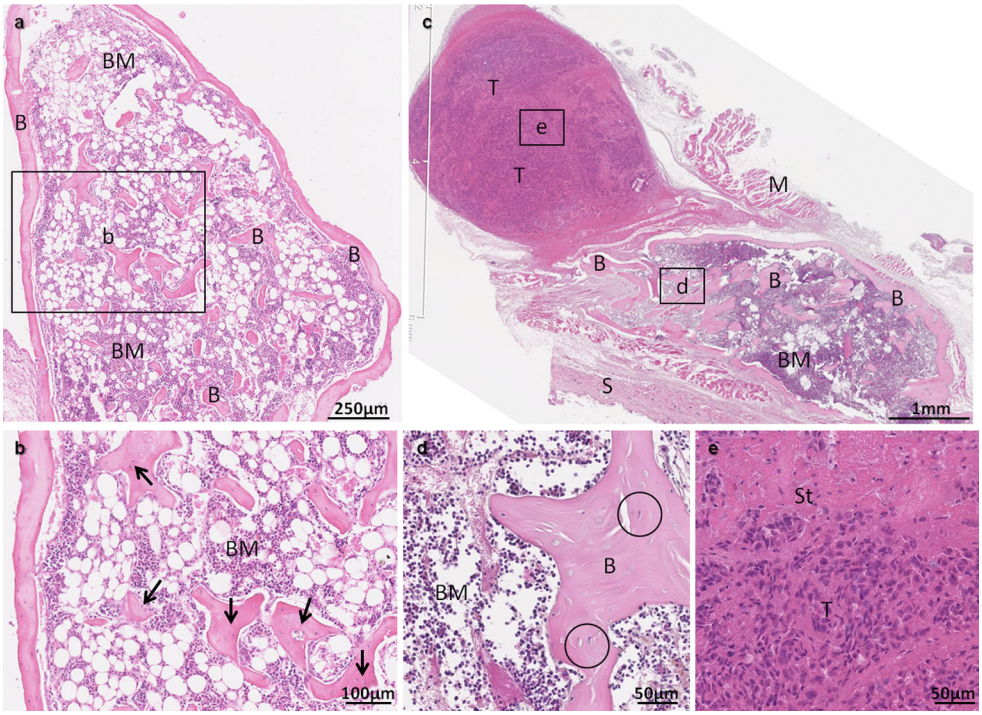

Fig. 3 Histological analyses (H&E) of control mice (*left panels*) and tumors in hTEBCs injected with LNCaP cells (*right panels*). **a** Overview of the hTEBC in the vehicle control mice at the 19 week end point, **b** Higher magnification of the boxed area in **a**; trabecular bone in the form of small islands was present in the bore of the hTEBC (*black arrows*) whereas cortical bone was surrounding the hTEBC forming a shell around it. Bone marrow (BM) was present in the woven and cortical bone area. **c** Overview of the hTEBC injected with LNCaP cells at the 19 week end point showing asymmetrical tumor growth, **d** Higher magnification of the implant area (*bone*); significant amount of new bone formation with bone marrow showing osteocytes in bone lacunae indicative of viable bone (*circles*) and **e** Higher magnification of the LNCaP tumor showing LNCaP cell morphology. *T* tumor, *B* bone, *BM* bone marrow, *M* muscle, *St* stroma, *S* skin

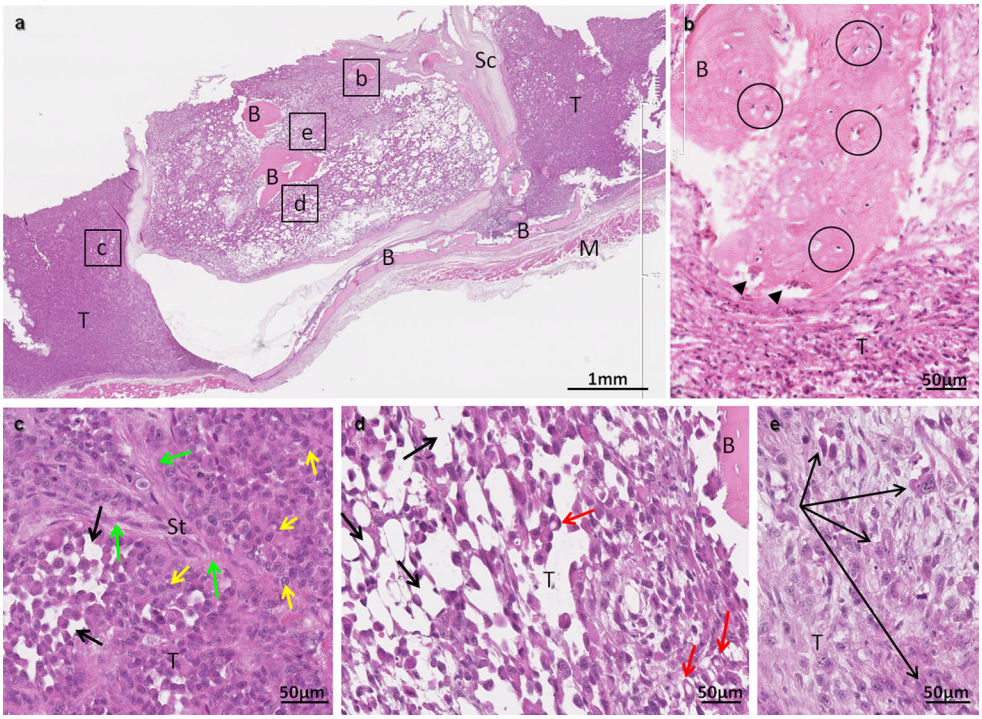

Fig. 4 Histological analyses (H&E) of tumors in hTEBCs injected with PC3 cells. **a** Overview of the hTEBC injected with PC3 cells at 19 week end point showing symmetrical tumor growth. **b–e** Higher magnifications of the boxed areas in **a**. **b** Osteoclasts within resorption pits (*black arrows*) at the bone–tumor interface. Empty circles showing osteocytes in bone lacunae indicative of viable bone, **c** Peripheral parts of the tumor showing PC3 tumor cells (*yellow arrows*) embedded in vacuolated (*black arrows*) and fibrous stroma (*green arrows*), **d** Central part of the tumor revealed vacuolated PC3 tumor cells (*red arrows*) and a vacuolated stroma (*black arrows*). Only very few bone islands were left. **e** Some PC3 tumor cells in the centre showed a spectrum of morphological features such as epithelial (*lowest black arrow*) and mesenchymal (*top black arrows*) phenotypes. *T* tumor, *B* bone, *Sc* scaffold, *M* muscle, *St* stroma

which staining intensity was visually scored by an experienced pathologist [30]. Figure 5f shows the mean PTHrP expression in hTEBC at the 19-week end point in the implant and tumor areas. The trend showed higher levels for PTHrP expression in PC3 tumors compared to LNCaP tumors in both tumor and implant areas (Fig. 5g–j).

Histological aspects of PC3 and LNCaP tumors within the hTEBC are shown in Figs. 3 and 4. Both PC3 and LNCaP cancer cell lines formed tumors in vivo with morphological aspects of large sheets of tumor cells and a small amount of stroma in the PC3 tumors and larger amount of stroma in the LNCaP tumors as it was reported in previous studies [31]. In hTEBCs injected with PC3 cells, tumor cells were occupying the bone marrow spaces. PC3 cells infiltrated the hTEBC and were in direct contact with newly formed bone. Necrosis was more severe in LNCaP than in PC3 tumors; necrosis was not observed in the control group (data not shown). Microvessel density as assessed on vWF staining in different areas showed that LNCaP tumor vessel density was significantly higher in hTEBC implants than in those injected with PC3 cells ($p < 0.001$) (Fig. 6a). Furthermore, it was observed that tumor blood vessels had abnormally formed networks and extended branches of endothelial cells. These features were particularly obvious in LNCaP tumors (Fig. 6b–e).

In both PC3 and LNCaP tumors a mild desmoplastic stromal response was observed. Tumor cells in LNCaP- and PC3-injected hTEBCs preserved their round cellular morphology in areas peripheral to the hTEBC (epithelial phenotype) (Figs. 3, 4). However, PC-3 cells exhibited two different morphological phenotypes in the central bone marrow spaces of the hTEBCs. In one area, PC3 tumor cells seemed to be vacuolated and were scattered in a vacuolated stroma (Fig. 4d). In the second area, PC3 tumor cells were more spindle shaped suggesting a mesenchymal phenotype (Fig. 4e). These cells expressed a high level of vimentin as compared to the round shaped peripheral PC3 cells, confirming some epithelial mesenchymal plasticity. LNCaP tumors were negative when immunostained for anti-vimentin (Fig. 7a–c). Strong E-cadherin expression was detected in the tumor area of LNCaP- and PC3-injected hTEBCs. However, E-cadherin expression was weaker in the implant areas of PC3-injected hTEBC in places in which PC3 tumor cells

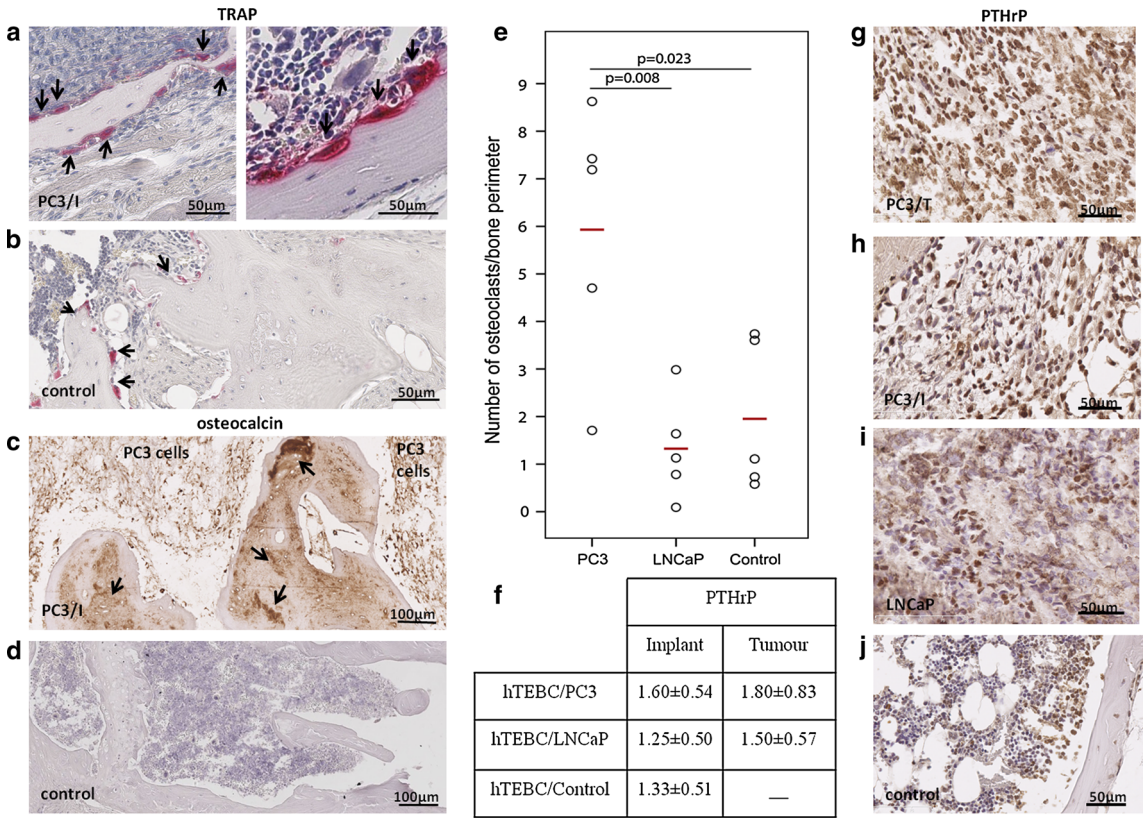

Fig. 5 PC3 cells recapitulate their osteolytic phenotype in hTEBCs. **a** Representative image from TRAP positive staining osteoclasts (*black arrows*) on the surface of a bone island in direct contact with the PC3 tumor (implant area: PC3/I), and **b** in a femur of a healthy age-matched mouse. **c** Immunohistochemical staining with anti human-osteocalcin of PC3-injected hTEBC (implant area: PC3/I), human specific osteocalcin expression (*black arrows*) in newly formed bone and PC3 cells. **d** No anti-human osteocalcin staining in a femur of a healthy age-matched mouse. **e** Number of osteoclasts per bone perimeter (TRAP staining); significant difference is indicated by a *horizontal bar* (*p* value). Means are indicated by *red lines* for each group ($n = 5$ per group). **f** Table of mean score of PTHrP staining in hTEBC tumor cells at 19 week end point. **g–j** Representative photomicrographs of the immunohistochemical staining with anti-PTHrP from **g** tumor area (*T*) of hTEBC injected with PC3 cells, **h** implant area (*I*) of hTEBC injected with PC3 cells, **i** hTEBC injected with LNCaP cells and **j** hTEBC in control mice. Differences in PTHrP expression were observed with the highest expression of PTHrP in the PC3 tumor area

showed a spectrum of morphological features of epithelial and mesenchymal phenotypes (Fig. 7d–f).

Discussion

Current in vivo models to study human PCa bone metastasis lack the level of complexity necessary to derive solid conclusions about the interactions between human cancer cells and the human bone microenvironment. Here we report a newly developed and validated bioengineered humanized mouse model that mimics the phenotype of bone lesions observed clinically in PCa. Injection of human cancer cells into the murine skeleton does not appropriately mimic the human tumor microenvironment and therefore it is very difficult to predict drug responses of a human tumor grown in a human patient [32]. Though mice share many genes and molecular pathways with humans, significant differences exist with regard to organ physiology and regulatory proteins [33]. Critical discrepancies may arise in the nature of the vasculature of the tumor as a result of altered interaction patterns between the human tumor and the extracellular matrix of the murine host. Therefore, in recent years it has become increasingly clear that novel animal models of human cancer that more closely recapitulate clinical conditions are required [34]. This need has prompted more and more researchers to humanize their models by the implantation of human bone into the murine host. Reports describing the biology of implanted human fetal bone fragments suggest that viability of the tissue could be maintained after implantation. However, the composition of fetal bone significantly differs from adult bone as the metaphysis and epiphysis consists mainly of hyaline cartilage [26]. Holzapfel et al. [6] could demonstrate that adult human bone chips without growth factor stimulation do not sufficiently mimic the biological

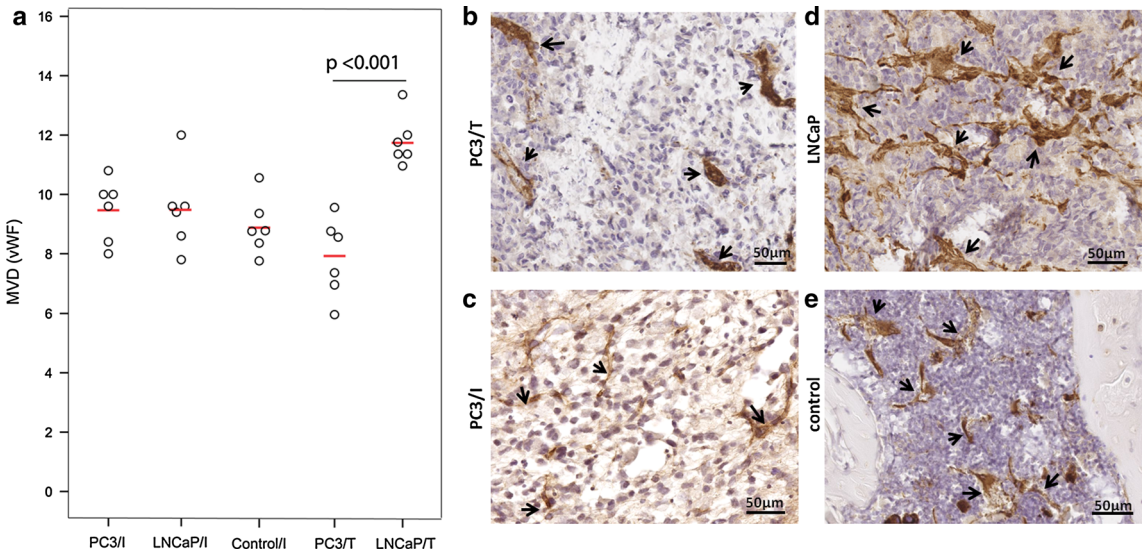

Fig. 6 Microvessel Density (MVD) measured by anti-vWF immunoreactivity. **a** Two different areas (*T* tumor only area, *I* implant area) of implanted hTEBC in mice injected with LNCaP and PC3 cells and vehicle control mice (no cancer) at 19 week end point were analyzed ($n = 6$ per group). Numbers are shown per field (area = 0.58 mm^2). Significant difference is indicated by a *horizontal bar* (*p* value). Means are indicated by *red lines* for each group. **b–e** Representative photomicrographs of the immunohistochemical staining with anti-vWF from **b** tumor area (*T*) of hTEBC injected with PC3 cells, **c** implant area (*I*) of hTEBC injected with PC3 cells, **d** hTEBC injected with LNCaP cells and **e** hTEBC in control mice. *Black arrows* label some of the positive blood vessels that were stained *brown*. It can clearly be seen that blood vessels are dilated and have an abnormal morphology by forming networks and extended branches. The number of blood vessels was higher in LNCaP tumors

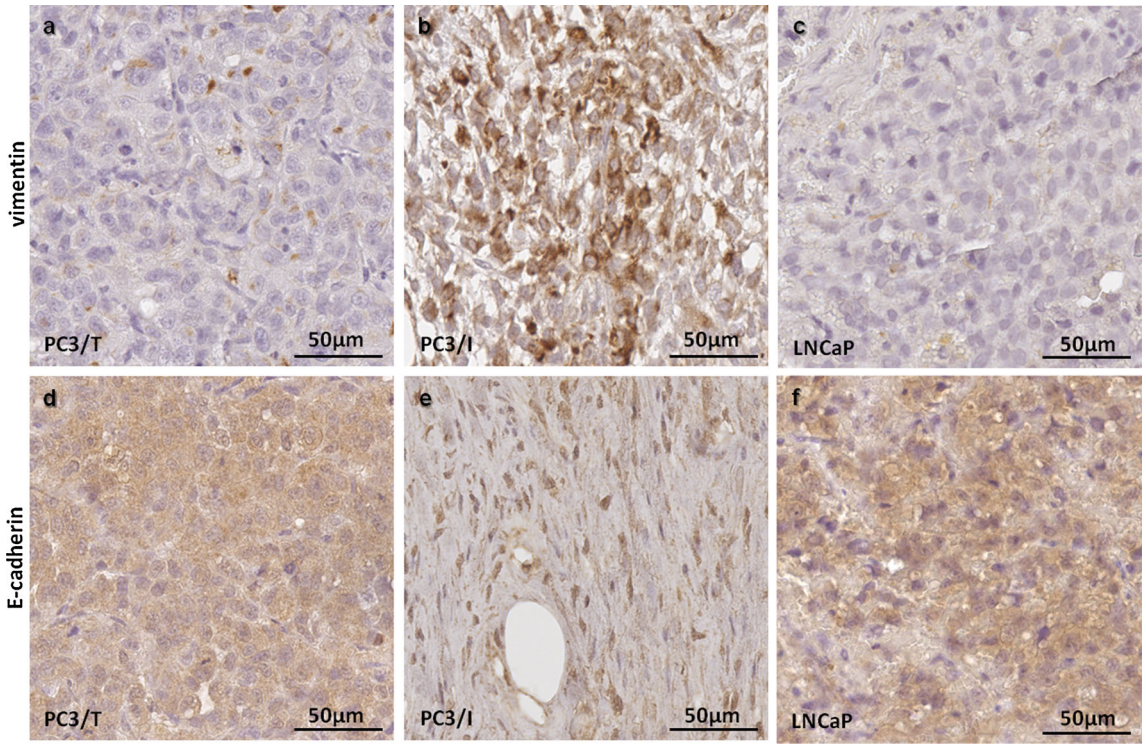

Fig. 7 Representative photomicrographs of the immunohistochemical staining with anti-vimentin (*top panel*) and anti-E-cadherin (*bottom panel*). **a** Tumor area and **b** Implant area of PC3-injected hTEBC; vimentin was highly expressed in the implant area of PC3-injected hTEBC where cells showed EMP phenotypic changes, **c** LNCaP tumors were negative for vimentin. **d** Tumor area and **e** Implant area of PC3-injected hTEBC, **f** LNCaP tumor; differences in E-cadherin expression, particularly down regulation of E-cadherin in implant areas of PC3-injected hTEBC, were observed

character of viable human bone as the implanted bone is poorly vascularized, necrotic and the trabecular spaces are filled with fat cells and fibrotic tissue.

Therefore, we have established a unique model to study species–specific interactions between human PCa cells and a humanized tissue-engineered organ bone. We could clearly show that the implantation of hTEBCs leads to the development of a vital and functional humanized bone organ in NOD/SCID mice. Mesenchymal cells within the newly formed bone were to a great extent of human origin, whereas the hematopoietic system was of murine origin. These results show that it is possible to engineer humanized bone which serves as a functional niche for endogenous hematopoietic cells.

After injection of human PCa cells into the constructs we were able to reproducibly recapitulate the growth pattern of human PCa cells in the humanized bone matrix. PC3 tumor cells interacted with the humanized construct while LNCaP tumor cells were not in direct contact with the humanized bone matrix. It could be suggested that PC3 and LNCaP tumor formation in the current study mimic the metastatic lesions from which they are originally derived; viz, PC3 cells are derived from a bone metastasis and LNCaP cells are derived from a lymph node metastasis [35–37]. PC3 cells were occupying the newly formed bone tissue. This result is consistent with studies reporting PC3 tumor growth in pre-implanted human bone chips [10, 38]. In contrast, in the current study, LNCaP cells did not grow in the newly-formed organ, a finding similar to a previous report in which tail vein injection of LNCaP cells in SCID mice did not result in any tumor formation in the pre-implanted human bone chip [20]. In a study of tail vein injection of PCa cells in NOD/SCID mice, PC3 cells metastasized to 65 % while LNCaP cells metastasized to 35 % of the pre-implanted human bone chips [10]. This indicated that although the take rate of LNCaP tumors was less than that of PC3 tumors, some LNCaP cells were still able to form tumors in the bone microenvironment. Although there is a dogma regarding dominant osteoblastic lesions developed by LNCaP cells, to our knowledge there are no studies to evaluate the amount of these osteoblastic lesions quantitatively before and after inoculation of this cancer cell line. It has been shown that intra-tibial injection of LNCaP cells resulted in mixed bone lesions, even so the extension of these lesions has not been specified [31]. Overall, this suggests that LNCaP cells might not be a good model for bone metastatic studies as previously described [6].

In the current study, within this humanized bone microenvironment, PC3 tumors showed a pronounced osteolytic response as confirmed via micro-CT, a large number of TRAP positive osteoclasts and resorption pits evident in histological sections. Thus, PCa tumors recapitulate their well-known phenotypic behavior and our results are in agreement with previous work in which PCa cells were injected into human fetal bone chips in a subcutaneous mouse model [11]. In the study by Podgorski et al. [11], PC3 cells induced significant osteolytic lesions such that 6 weeks after injection, bone fragments could no longer be observed in most cases. Although LNCaP cells did not induce any significant bone lesions, bone cells were proliferating along the newly formed bone as noted from histological analysis and the bone mass was preserved.

PTHrP is commonly expressed in human PCa bone metastases and is known to play important roles in bone remodeling [29]. PTHrP is a central mediator of osteolysis hypercalcemia of malignancy. PTHrP secreted by PCa cells is suspected to activate osteoclasts in osteolytic PCa bone metastasis that could lead to skeletal invasiveness, bone pain and pathological fractures [17]. In the present study there was a trend towards a higher PTHrP expression in PC3-compared to LNCaP-formed tumors (in the tumor area). This coincides with Wu et al.'s [39] observation that PTHrP expression in PC3 cells was higher than in LNCaP cells. It is unknown whether the higher level of expression of PTHrP in PC3 cells is related to the bone microenvironment of the hTEBC. However, in another study conducted by us, PC3 and LNCaP cells cultured on a mineralized human osteoblast matrix showed that LNCaP cells had a very low PTHrP expression whereas PC3 cells expressed high levels of PTHrP when cultured on the osteoblast matrix [17]. Therefore, it can be concluded that higher PTHrP expression in PC3 tumors in this hTEBC bone microenvironment could be consistent with the osteolytic phenotype of PC3 cells previously described [40].

Higher numbers of large and dilated blood vessels observed in LNCaP compared to PC3 tumors, as well as leaky blood vessels, explains the macroscopic appearance of LNCaP tumors. Abnormally formed blood vessel networks and extended branches of their endothelial cells in the current model recapitulate the malignant tumor vascularization pattern seen in clinical studies where tumor vessels are highly fragile and leaky [41]. In addition, in the current study, there was a higher degree of necrosis in LNCaP tumors compared with PC3 tumors (data not shown) which may be due to local hypoxia. It has been reported that hypoxia induces angiogenesis in tumors [42]. This presumably explains the higher number of blood vessels in LNCaP tumors compared with PC3 tumors and emphasizes the clinical utility of our model.

To our knowledge this project is the first study showing both epithelial and mesenchymal phenotypes of PC3 cells in a tumor environment indicative of epithelial to mesenchymal plasticity (EMP) [43] in PC3 cells although the precise mechanisms or underlying molecular pathways were not studied here. In certain areas, PC3 cells displayed

a loss of surface E-cadherin and showed an upregulation of vimentin, a mesenchymal cell marker. As described previously, the PC3 cell line is a highly aggressive malignant PCa cell line derived from a bone metastasis [35–37]. Our results support the hypothesis that EMP contributes to tumor aggressiveness [44]. It has been reported that EMP occurs in a number of human cancers, including PCa [45–50] particularly at the invasive edge of tumors. In this study, it was notable that these EMP changes only occurred in PC3 cells within the newly formed bone. Hence, the bone microenvironment should be considered a key contributor to this plasticity. Another interesting observation was the vacuolated PC3 cells. This histopathological observation may be interpreted as a cellular distress however the reasons underlying these cellular changes are unknown.

Our new approach provides significant advantages over traditionally used xenograft models of bone metastasis. This model allows the control of shape, size and porosity of the implant. Furthermore, tissue-engineered bone constructs are predictably reproducible, consistent and not limited in supply like fetal or adult human bone. The amount and viability of cells seeded onto the construct can be monitored before implantation into the host. As only cellular components are transferred, there is a reduced risk of infectious disease transmission as compared to the implantation of bone [6].

In this study we were able to recapitulate the entire sequence of events that occur during endochondral bone formation in a clinical setting from single cells (hOBs seeded on scaffolds), to cartilage and finally to bone formation with the presence of bone marrow. This model enables us to recapitulate the physiology of a functional organ bone not only with its bone matrix but also with its hematopoietic system. Of note, the hematopoietic system in our model is of murine origin and the human PCa cells are influenced by growth factors from both the murine host and the transplanted human cell complex.

In future studies hTEBCs could be used as a homing site for PCa cells introduced into the circulation by tail vein, intra-cardiac or orthotopic injection, which is lacking in most metastasis models and represents a critical potential for studying tumor cell dormancy and early metastasis implantation. In addition, this in vivo model could be used to address a range of questions relevant to the biology of PCa bone metastasis, which were beyond the scope of this project. The model provides an exciting opportunity to dissect the role of proteases and other factors in the bone microenvironment subsequent to the arrival of cancer cells. One of the highlights of this study was the presence of bone marrow in the hTEBCs. To investigate the interactions of human PCa cells not only with human bone cells but also with human bone marrow cells, the model may be extended by including more human components, such as human hematopoietic stem cells to study the interplay between cancer cells and a humanized immune system.

Overall, improved models of PCa metastasis such as that reported here will allow a better understanding of the complex interactions between PCa cells and the bone microenvironment and ultimately make it possible to test novel cancer therapeutics.

Acknowledgments The work presented by the authors is supported by the Prostate Cancer Foundation of Australia, the National Health & Medical Research Council (NHMRC) Fellowship Grant, the Australian Research Council and the German Research Foundation (DFG HO 5068/1-1). We thank Baxter Healthcare International and Olympus Biotech for providing fibrin glue and rhBMP-7, respectively.

Conflict of interest The authors declare that they have no conflict of interest.

References

1. Siegel R et al (2012) Cancer treatment and survivorship statistics, 2012. CA Cancer J Clin 62(4):220–241
2. Ferlay J, Shin HR, Bray F, Forman D, Mathers C, Parkin DM (2010) GLOBOCAN 2008 v2.0, cancer incidence and mortality worldwide: IARC CancerBase No. 10. In: Cancer IAfRo. IARC, Lyon
3. Rades D, Schild SE, Abrahm JL (2010) Treatment of painful bone metastases. Nat Rev Clin Oncol 7(4):220–229
4. Singh AS, Figg WD (2005) In vivo models of prostate cancer metastasis to bone. J Urol 174(3):820–826
5. Pilge H et al (2011) Diagnostics and therapy of spinal metastases. Orthopade 40(2):185–193
6. Holzapfel BM et al (2013) Humanised xenograft models of bone metastasis revisited: novel insights into species–specific mechanisms of cancer cell osteotropism. Cancer Metastasis Rev 32(1–2):129–145
7. Corey E et al (2002) Establishment and characterization of osseous prostate cancer models: intra-tibial injection of human prostate cancer cells. Prostate 52(1):20–33
8. Fizazi K et al (2003) Prostate cancer cells-osteoblast interaction shifts expression of growth/survival-related genes in prostate cancer and reduces expression of osteoprotegerin in osteoblasts. Clin Cancer Res 9(7):2587–2597
9. Yonou H et al (2003) Osteoprotegerin/osteoclastogenesis inhibitory factor decreases human prostate cancer burden in human adult bone implanted into nonobese diabetic/severe combined immunodeficient mice. Cancer Res 63(9):2096–2102
10. Yonou H et al (2001) Establishment of a novel species- and tissue-specific metastasis model of human prostate cancer in humanized non-obese diabetic/severe combined immunodeficient mice engrafted with human adult lung and bone. Cancer Res 61(5):2177–2182
11. Podgorski I et al (2005) Bone microenvironment modulates expression and activity of cathepsin B in prostate cancer. Neoplasia 7(3):207–223
12. Nemeth JA et al (2000) Persistence of human vascular endothelium in experimental human prostate cancer bone tumors. Clin Exp Metastasis 18(3):231–237

13. Storey JA, Torti FM (2007) Bone metastases in prostate cancer: a targeted approach. Curr Opin Oncol 19(3):254–258
14. Hung TT et al (2011) Zoledronic acid preserves bone structure and increases survival but does not limit tumour incidence in a prostate cancer bone metastasis model. PLoS One 6(5):e19389
15. Kolambkar YM et al (2010) Colonization and osteogenic differentiation of different stem cell sources on electrospun nanofiber meshes. Tissue Eng A 16(10):3219–3230
16. Vaquette C et al (2013) Effect of culture conditions and calcium phosphate coating on ectopic bone formation. Biomaterials 34(22):5538–5551
17. Reichert JC et al (2010) Mineralized human primary osteoblast matrices as a model system to analyse interactions of prostate cancer cells with the bone microenvironment. Biomaterials 31(31):7928–7936
18. Sieh S et al (2010) Interactions between human osteoblasts and prostate cancer cells in a novel 3D in vitro model. Organogenesis 6(3):181–188
19. Reichert JC et al (2010) Ovine bone- and marrow-derived progenitor cells and their potential for scaffold-based bone tissue engineering applications in vitro and in vivo. J Tissue Eng Regen Med 4(7):565–576
20. Nemeth JA et al (1999) Severe combined immunodeficient-hu model of human prostate cancer metastasis to human bone. Cancer Res 59(8):1987–1993
21. Erlebacher A, Derynck R (1996) Increased expression of TGF-beta 2 in osteoblasts results in an osteoporosis-like phenotype. J Cell Biol 132(1–2):195–210
22. Gray DR et al (2004) Short-term human prostate primary xenografts: an in vivo model of human prostate cancer vasculature and angiogenesis. Cancer Res 64(5):1712–1721
23. Offersen BV et al (2002) Comparison of methods of microvascular staining and quantification in prostate carcinoma: relevance to prognosis. APMIS 110(2):177–185
24. de la Taille A et al (2000) Microvessel density as a predictor of PSA recurrence after radical prostatectomy. A comparison of CD34 and CD31. Am J Clin Pathol 113(4):555–562
25. Berner A et al (2012) Biomimetic tubular nanofiber mesh and platelet rich plasma-mediated delivery of BMP-7 for large bone defect regeneration. Cell Tissue Res 347(3):603–612
26. Roberts S et al (2009) Immunohistochemical study of collagen types I and II and procollagen IIA in human cartilage repair tissue following autologous chondrocyte implantation. Knee 16(5):398–404
27. Price PA et al (1976) Characterization of a gamma-carboxyglutamic acid-containing protein from bone. Proc Natl Acad Sci USA 73(5):1147–1151
28. Yeung F et al (2002) Regulation of human osteocalcin promoter in hormone-independent human prostate cancer cells. J Biol Chem 277(4):2468–2476
29. Liao J et al (2008) Tumor expressed PTHrP facilitates prostate cancer-induced osteoblastic lesions. Int J Cancer 123(10): 2267–2278
30. Cox ME et al (2009) Insulin receptor expression by human prostate cancers. Prostate 69(1):33–40
31. Corey E et al (2002) Establishment and characterization of osseous prostate cancer models: intra-tibial injection of human prostate cancer cells. Prostate 52(1):20–33
32. Richmond A, Su Y (2008) Mouse xenograft models vs GEM models for human cancer therapeutics. Dis Model Mech 1(2–3): 78–82
33. Dreesen O, Brivanlou AH (2007) Signaling pathways in cancer and embryonic stem cells. Stem Cell Rev 3(1):7–17
34. Meeting Summary (2012) Improving animal models for regenerative medicine. In: NIH symposium, May 23–24, Bethesda. http://dpcpsi.nih.gov/orip/documents/summary_of_the_improving_animal_models.pdf. Accessed 2 Feb 2013
35. Chu K et al (2008) Cadherin-11 promotes the metastasis of prostate cancer cells to bone. Mol Cancer Res (MCR) 6(8): 1259–1267
36. Sardana G et al (2008) Proteomic analysis of conditioned media from the PC3, LNCaP, and 22Rv1 prostate cancer cell lines: discovery and validation of candidate prostate cancer biomarkers. J Proteome Res 7(8):3329–3338
37. Tai S et al (2011) PC3 is a cell line characteristic of prostatic small cell carcinoma. Prostate 71(15):1668–1679
38. Nemeth JA et al (2002) Matrix metalloproteinase activity, bone matrix turnover, and tumor cell proliferation in prostate cancer bone metastasis. J Natl Cancer Inst 94(1):17–25
39. Wu G et al (1998) Characterization of the cell-specific expression of parathyroid hormone-related protein in normal and neoplastic prostate tissue. Urology 51(5A Suppl):110–120
40. Raheem O et al (2011) A novel patient-derived intra-femoral xenograft model of bone metastatic prostate cancer that recapitulates mixed osteolytic and osteoblastic lesions. J Transl Med 9:185
41. Brown JM, Wilson WR (2004) Exploiting tumour hypoxia in cancer treatment. Nat Rev Cancer 4(6):437–447
42. Fernandez A et al (2001) Angiogenic potential of prostate carcinoma cells overexpressing bcl-2. J Natl Cancer Inst 93(3): 208–213
43. Haviv I, Thompson EW (2012) Soiling the seed: microenvironment and epithelial mesenchymal plasticity. Cancer Microenviron 5(1):1–3
44. Kong D et al (2011) Cancer stem cells and epithelial-to-mesenchymal transition (EMT)-phenotypic cells: are they cousins or twins? Cancers 3(1):716–729
45. Chung LW et al (2006) Stromal-epithelial interaction in prostate cancer progression. Clin Genitourin Cancer 5(2):162–170
46. Hugo H et al (2007) Epithelial–mesenchymal and mesenchymal–epithelial transitions in carcinoma progression. J Cell Physiol 213(2):374–383
47. Zhau HE et al (2008) Epithelial to mesenchymal transition (EMT) in human prostate cancer: lessons learned from ARCaP model. Clin Exp Metastasis 25(6):601–610
48. Yates CC et al (2007) Co-culturing human prostate carcinoma cells with hepatocytes leads to increased expression of E-cadherin. Br J Cancer 96(8):1246–1252
49. Said NA, Williams ED (2011) Growth factors in induction of epithelial-mesenchymal transition and metastasis. Cells Tissues Organs 193(1–2):85–97
50. Lue HW et al (2011) LIV-1 promotes prostate cancer epithelial-to-mesenchymal transition and metastasis through HB-EGF shedding and EGFR-mediated ERK signaling. PLoS One 6(11): e27720